ACTIVE CONTOURS BASED ON WEIGHTED GRADIENT VECTOR FLOW AND BALLOON FORCES FOR MEDICAL IMAGE SEGMENTATION

Alaa Khadidos[1,2], Victor Sanchez[1] and Chang-Tsun Li[1]

[1]Department of Computer Science, University of Warwick, UK
[2]Faculty of Computing and Information Technology, King Abdulaziz University, Jeddah, Saudi Arabia

ABSTRACT

Active contours, or snakes, have been widely used for image segmentation purposes. However, high noise sensitivity and poor performance over weak edges are the most acute issues that hinder the segmentation accuracy of these curves, particularly in medical images. In order to overcome these issues, we propose a novel external force that integrates gradient vector flow (GVF) field forces and balloon forces based on a weighting factor computed according to local image features. The proposed external force reduces noise sensitivity, improves performance over weak edges and allows initialization with a single manually selected point. We evaluate the proposed external force for segmentation of various regions on real MRI and CT slices. Evaluation results show that the proposed approach leads to more accurate segmentation than snakes using traditional external forces.

Index Terms— Active contours, gradient vector flow (GVF), balloon forces, medical image segmentation.

1. INTRODUCTION

Since first introduced by Kass et al. [1], substantial work on parametric active contours, or snakes, has been achieved for their application in image segmentation, including medical images [2–5]. The main principle behind snakes is to model the movement of a dynamic curve towards an object's boundary under the influence of internal and external forces. Internal forces control the smoothness of the curve, while external forces lead the curve to the boundary until convergence is achieved.

Due to the wide variety of object shapes, there are still many situations where snakes fail to converge to the desired boundary, especially when the amount of image clutter and noise is high [6]. In such cases, segmentation accuracy may be improved by manually initializing the curve very close to the object's boundary. Depending on the region to be segmented, this initialization process may require the selection of several initial points or snake elements, which may become a tedious and error-prone process, particularly in medical images.

Many researchers have proposed solutions to address the issue of convergence [2,7,8]. The work of Cohen [7] represents one of the initial solutions, which consists of employing an external force to guide the snake to the object's boundary in a similar way a balloon inflates or deflates. These *balloon forces* have been proved to improve convergence when the snake is initialized far from the desired boundary. However, if the strength of the balloon forces is too high, the snake may not detect weak edges resulting in snake leakages. Another important solution is the one proposed by Xu et al., which introduces the gradient vector flow (GVF) field as an external force. The GVF force increases the capture range of the snake, allowing it to conform to concave boundaries. This external force, however, may still fail to accurately converge to the desired boundary if the levels of noise in the image are high [9].

After the introduction of the GVF force, important work has been done to further improve the convergence of snakes. In [6], Zhu et al. propose the gradient and direction vector flow (G&DVF) external force, which integrates the GVF field and prior directional information manually provided by the user. In [10], Qin et al. propose a new external force called component-normalized generalized-GVF (CN-GGVF), which improves the detection of concave regions and long and thin indentations. Yao et al. [11] propose the sigmoid gradient vector flow (SGVF) external force, which is obtained by convolving the original image with a sigmoid function before computing the GVF field. This external force, which features a reduced noise sensitivity, is capable of minimizing snake leakages.

Other important solutions that improve convergence of snakes for medical image segmentation include the work in [4, 5]. In [4], Wu et al. propose the gradient vector convolution (GVC) field as an external force, which is calculated by convolving the gradient map of an image with a defined kernel. This method is, however, limited to segmenting specific anatomical regions such as the left ventricle in cardiac MRI. Zhang et al. [5] propose improvements to the GVF snake by using a combination of balloon and tangential forces. This method is, however, very sensitive to a set of parameters.

The majority of external forces proposed in [4–6, 10, 11] still require that the initial snake be placed close to the desired boundary to improve segmentation accuracy, especially in cases where the amount of image clutter and noise is high, such as in medical images. This inevitably involves manually selecting several initial snake elements. Moreover, they may still fail to accurately drive the snake to the desired boundary around weak edges [12].

In this work, we propose a new external force that combines the advantages of balloon and GVF forces. Specifically, we employ balloon forces to guide the snake to the object's boundary even in the presence of image clutter and noise; while we employ GVF forces to improve convergence to the object's boundary even around weak edges. We control the influence of these two types of forces on the snake's movement by using a weighting function based on local image features. The proposed external force minimizes snake leakages and considerably reduces the number of initial snake elements, making suitable for segmentation of medical images with little manual intervention.

The rest of the paper is organized as follows. Section 2 reviews the basic concepts of snakes. Our proposed external force is detailed in Section 3. Experimental results for segmentation of real medical images are presented in Section 4. Finally, we draw conclusions in Section 5.

2. BACKGROUND

A snake is a curve $C(s) = [x(s), y(s)], s \in [0, 1]$, that evolves to an object's boundary by minimizing the following energy function:

$$E_S(C) = \frac{1}{2}\int_0^1 (\alpha|C'(s)|^2 + \beta|C''(s)|^2)ds + \int_0^1 E_{ext}(C(s))ds \quad (1)$$

where α and β are weighting parameters that control the snake's tension and rigidity, respectively. The first integrand in Eq. (1) is referred to as the internal energy, which controls the smoothness of C, while the second integrand is referred to as the external energy, which attracts C towards the object's boundary. The external energy is usually defined as the negative intensity of the image edge map f, i.e., $E_{ext}(x, y) = -f(x, y)$, which is usually computed by:

$$f(x, y) = |\nabla [G_\sigma(x, y) * I(x, y)]|^2 \quad (2)$$

where G_σ denotes a 2D Gaussian filter with standard deviation σ, $*$ denotes a linear convolution, ∇ denotes the gradient operator and $I(x, y)$ denotes the image. The minimization of E_S can be achieved by evolving the snake dynamically as a function of parameter s and artificial time t as follows:

$$C(s, t) = \left[\alpha C''(s, t) - \beta C''''(s, t)\right] - \nabla E_{ext} \quad (3)$$

where the first term and the second term are called the internal force, F_{internal}, and the external force, $F_{external}$, respectively.

External forces can be divided into dynamic forces and static forces [2]. Dynamic forces, e.g., balloon forces, depend on the snake itself and change as the snake deforms. Static forces, e.g., GVF forces, are computed from the image and do not change as the snake deforms.

Balloon forces are computed iteratively and may have an inflation or deflation effect on the snake depending on the snake's initial position with respect to the desired boundary. These forces are represented as:

$$F_{balloon} = kn(s) \quad (4)$$

where $n(s)$ is a unit vector normal to the snake at snake element C_n, and k is the force strength. The sign of k is responsible for inflation (+) or deflation (-).

GVF forces are derived from the diffusion of the gradient vectors of the image edge map. Let $\mathrm{v}(x, y) = [u(x, y), \nu(x, y)]$ denote the GVF field, which is set to minimize the following energy function:

$$E_{GVF}(\mathrm{v}) = \iint \mu|\nabla \mathrm{v}|^2 + |\nabla f|^2|\mathrm{v} - \nabla f|^2 dxdy \quad (5)$$

The first term in Eq. (5) is used to smooth the vector field v, which has the main effect of increasing the capture range of the force field, where μ is a smoothness regularization parameter. The second term is the data fidelity term that makes v equal to the gradient vector of the edge map (∇f) where ($|\nabla f|$) is relatively large, and thus preserves edge information. The GVF force is then given as ($F_{GVF} = \mathrm{v}(x, y)$).

3. PROPOSED EXTERNAL FORCE

The proposed external force is a weighted combination of balloon and GVF forces and aims at exploiting the advantages of each of these two types of forces. As described in section 2, the computation of the GVF force requires the computation of the gradient vector of the edge map, ∇f. In this work, the edge map $f(x, y)$ is computed by first calculating the eigenvalues and eigenvectors of the 2×2 Hessian matrix $HM_{x,y,L}$, for each pixel at position (x, y). The elements of $HM_{x,y,L}$ are the coefficients of the three detail sub-bands of the stationary wavelet transform (SWT) decomposition of the image at level L, as follows:

$$HM_{x,y,L} = \begin{bmatrix} |V_{x,y,L}| & |D_{x,y,L}| \\ |D_{x,y,L}| & |H_{x,y,L}| \end{bmatrix} \quad (6)$$

where $V_{x,y,L}$, $H_{x,y,L}$ and $D_{x,y,L}$ are the coefficients of the vertical, horizontal and diagonal detail sub-bands, respectively, at pixel position (x, y) and decomposition level L. We use the largest absolute eigenvalue of $HM_{x,y,L}$, whose eigenvector represents the direction of highest curvature, as the intensity value of the edge information at position (x, y), so that $f(x, y) = \max(|e1_{x,y}|, |e2_{x,y}|)$, where $e1_{x,y}$ and $e2_{x,y}$ denote the two eigenvalues associated with $HM_{x,y,L}$. We normalize $f(x, y)$ to the range $[0, 1]$.

The proposed external force is then defined as follows:

$$F_{external} = (F_{Balloon} * (1 - \Omega)) + (F_{GVF} * \Omega) \quad (7)$$

where F_{GVF} and $F_{Balloon}$ denote the GVF force and balloon force, respectively, and $\Omega \in [0, 1]$, is a weighting factor given by:

$$\Omega = \bar{h}^{(1-(\bar{AD}-\varepsilon))} \quad (8)$$

where $\bar{h} \in [0, 1]$ denotes the average value of $f(x, y)$ over a semi-circular region S centered at each snake element, and $\bar{AD} \in [0, 1]$ is the angular difference between the direction of the balloon force and the average direction of the GVF force field over a cone-shaped region T centered at each snake element. $\bar{AD} = 0$ represents 0 radians, while $\bar{AD} = 1$ represents π radians. The constant $\varepsilon = 0.001$ is used to prevent power by zero when $\bar{AD} = 1$. For each snake element at position (x, y), $\bar{h}$ is calculated as follows:

$$\bar{h}(x, y) = \frac{1}{N}\sum_{(i,j)\in S} h(i, j) \quad (9)$$

where N is the number of edge map pixels located in region S and h is the edge intensity at position (i, j), as illustrated in Fig. 1.

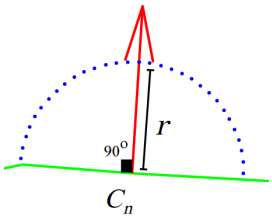

Fig. 1: Region S for snake element C_n. The snake is represented in green. The red arrow represents the direction of the balloon force which is normal to the snake at element C_n. The blue doted line represents region S of radius r.

For each snake element at position (x, y), $\bar{AD}$ is calculated as follows:

$$\bar{AD}(x, y) = \frac{1}{M * \pi}\sum_{(i,j)\in T} \theta(i, j) \quad (10)$$

where M is the number of GVF field vectors in region T, θ is the angle between the GVF field vector at point (i, j) and the balloon force

vector for snake element C_n at position (x, y). Region $T(x, y, sl, \varphi)$ is defined by a cone shape with its vertex in (x, y), as illustrated in Fig. 2. Note that a cone-shaped region was chosen as opposed to a semi-circular region, such as region S, for two reasons. First, it allows analyzing the region located far from the snake element, which provides a better insight of the direction of the GVF field than the region close to the snake element. Second, it reduces the number of calculations since there are fewer points in total than a semi-circular region of equivalent size.

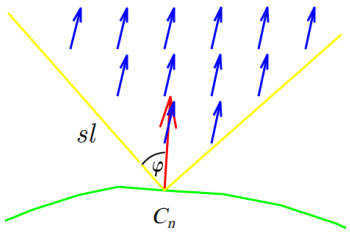

Fig. 2: Region T for snake element C_n. The snake is represented in green. The red arrow represents the direction of the balloon force, which is normal to the snake at element C_n. Blue arrows represent the GVF field vectors within region T.

Note that the weighting function in Eq. (8) assigns different priorities to balloon and GVF forces according to local image features. These features are the average amount of edge information ($\bar{h}$) and average direction of the GVF field ($\bar{AD}$). It is important to mention that the simplest possible method to control the influence of balloon and GVF forces on the snake's movement is to use a thresholding approach based on $\bar{h}$ and $\bar{AD}$ values. However, the use of continuous functions, such as the one in Eq. (8), where no hard decision is required, usually leads to better results [13]. Fig. 3 shows the plot of Eq. (8) for various values of $\bar{AD}$. It can be seen that Ω approaches 0 for small $\bar{h}$ values regardless of the $\bar{AD}$ value, i.e., when the snake is located in a smooth region. In this case, balloon forces are the main acting external forces driving the snake close to the object's boundary. It can also be seen that Ω approaches 1 in a linear fashion as $\bar{h}$ and $\bar{AD}$ increase, i.e., when the snake is located in a non-smooth region and its normal direction of growth does not coincide with the local average direction of the GVF field. In this case, GVF forces tend to be the main acting external forces, helping the snake conform to the object's boundary.

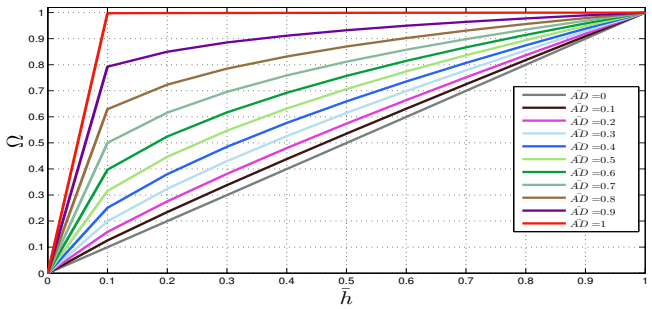

Fig. 3: Value of Ω for different values of $\bar{h}$ and $\bar{AD}$.

Therefore, Ω allows the snake to deform in smooth areas even if its normal direction of growth is opposite to the GVF force. This is particularly useful to initialize the snake with a very limited number of snake elements located far from the desired boundary. Fig. 4(a) and 4(b) illustrate this case, where Ω approaches 0. Weight Ω also minimizes snake leakages around weak edges by averaging the amount of edge information and the direction of the GVF field over

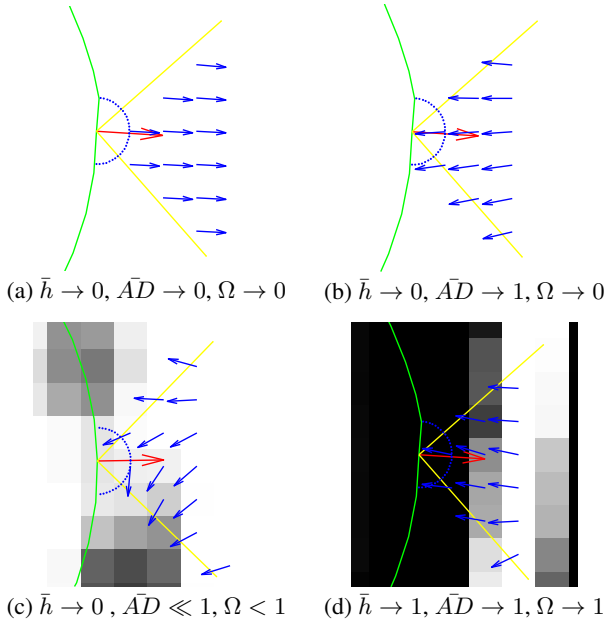

(a) $\bar{h} \to 0$, $\bar{AD} \to 0$, $\Omega \to 0$ (b) $\bar{h} \to 0$, $\bar{AD} \to 1$, $\Omega \to 0$

(c) $\bar{h} \to 0$, $\bar{AD} \ll 1$, $\Omega < 1$ (d) $\bar{h} \to 1$, $\bar{AD} \to 1$, $\Omega \to 1$

Fig. 4: Direction of the GVF field within region T for different cases where the average amount of edge information ($\bar{h}$) varies within region S (the snake is represented in green and non-white pixels represent strong edge information). (a) The direction of the GVF field is similar to the normal direction of growth of the snake (red). (b) The direction of the GVF field is opposite to the normal direction of growth of the snake. (c) The direction of the GVF force field around weak edges. (d) The direction of the GVF force field around strong edges.

regions S and T, respectively. This is illustrated in Fig. 4(c), where the value of Ω slowly approaches 1. Finally, Ω allows the snake to conform to the desired boundary by assigning a higher weight to the GVF force when edges are encountered. This is illustrated in Fig. 4(d), where the value of Ω approaches 1.

4. EXPERIMENTAL RESULTS

In this section, we present several experiments on real slices of MRI and CT sequences to evaluate the performance of the proposed external force compared to snakes using three different external forces: a) GVF force exclusively [2], b) balloon and image gradient (BGrad) forces [10], and c) balloon or GVF forces based on thresholding (BGVFT). In method (c), the external force is either balloon or GVF based on the value of $\bar{h}$, which is computed as described in section 3.

In our experiments, images are preprocessed using histogram equalization to enhance edges. The edge map is computed as described in section 3 using the Haar filter with $L = 3$ levels of decomposition. We use a value of $\alpha = 0$ and $\beta = 10$ to control the smoothness of the snake, and a value of $\mu = 0.2$ for the regularization parameter to compute the GVF field, as suggested in [2]. For our proposed external force, we use a radius $r = 1$ pixels for region S, an angle $\varphi = 45^o$ and $sl = 5$ pixels for region T. These values provide the best trade-off between capturing enough information about local image features and computational complexity. In all experiments, the snake is placed inside the desired region by manually selecting a single position. This single position is used as the center of an initial circular snake with a radius of 10 pixels.

Table 1: Detection accuracy of snakes using various external forces.

Exp.	GVF		BGrad		BGVFT		Proposed approach		No. iterations
	DSC	JC	DSC	JC	DSC	JC	DSC	JC	
1	0.934	0.877	0.902	0.822	0.894	0.809	**0.945**	**0.889**	13
2	0.947	0.900	0.919	0.850	0.916	0.845	**0.951**	**0.913**	13
3	0.931	0.872	0.886	0.796	0.922	0.855	**0.948**	**0.902**	14
4	0.936	0.880	0.903	0.824	0.917	0.847	**0.958**	**0.919**	15
5	0.929	0.868	0.903	0.824	0.925	0.861	**0.954**	**0.913**	16
6	0.099	0.052	0.852	0.743	**0.942**	**0.890**	0.932	0.872	44
7	0.026	0.012	0.630	0.460	**0.955**	**0.915**	0.926	0.862	101
8	0.954	0.913	0.884	0.792	0.905	0.826	**0.950**	**0.904**	13
9	0.924	0.859	0.919	0.851	0.896	0.812	**0.939**	**0.886**	8
10	0.856	0.748	0.852	0.742	**0.894**	**0.808**	0.857	0.750	27

Note that when computing the edge map $f(x, y)$ as described in section 3, the position of edges shifts by a number of pixels from their actual position in the original image. This shifting effect is a consequence of the redundant properties of the SWT and depends on the size of the filter [14, 15]. The amount of shifting Λ_L, in pixels locations, for L levels of decomposition using the Haar filter is given as follows:

$$\Lambda_L = \sum_{\ell=1}^{L} \Delta_{\ell-1:\ell} \tag{11}$$

$$\Delta_{L-1:L} = 2^{(L-3)} \times (d_0^{Lo} + 3d_0^{Hi} - 4) \tag{12}$$

where d_0^{Lo} and d_0^{Hi} denote the size of the low pass and high pass filters, respectively. For the Haar filter, $d_0^{Lo} = d_0^{Hi} = 2$. Therefore, the position of the final snake is shifted back according to Eq. (11) in order to correctly position the snake on the desired boundary in the original image.

The detection accuracy of the evaluated external forces is measured by the Dice similarity coefficient (DSC) [16] and Jaccard coefficient (JC) [17] using manually annotated ground truth. The values of DSC and JC are within the range $[0, 1]$, where 1 indicates identical overlap and 0 indicates no overlap between regions inside the boundaries. Table 1 tabulates the DSC and JC values for different regions of MRI and CT slices. The number of iterations is equal for all evaluated external forces and is set to the number of iterations required by our proposed external force to achieve convergence. Experiments 1-3 represent three different regions on an MRI slice of a spinal cord, experiments 4 and 5 represent two regions on an MRI slice of a pelvis, experiments 6 and 7 represent two regions on an MRI slice of a knee, experiment 8 represents one region on a CT slice of a skull, and experiments 9 and 10 represent two regions on a CT slice of a spinal cord.

Results in Table 1 show that our approach achieves the highest accuracy for the majority of experiments. It is important to note that in some cases, the BGVFT snake achieves higher DCS and JC values than our approach for the same number of iterations (see experiments 6,7,10). In these cases, the selected threshold for the BGVFT snake effectively switches between GVF and balloon forces. However, note that the BGVFT does not converge in the tabulated number of iterations. More iterations may cause snake leakage in the BGVFT snake, unlike our approach which achieves convergence in less iterations and detects the boundary with high accuracy by automatically weighting the GVF and balloon forces according to local image features. Visual results are shown in Fig. 5. The GVF snake, which is represented in yellow, conforms to the desired boundary in most of the depicted cases. However, for the region in Fig. 5 (a), this snake completely fails mainly due to the fact that the snake is initialized far from the boundary using a relatively small initial curve. Although the capture range of the GVF force is in general large, the direction of the GVF field around such small initial snakes may not point towards the desired boundary due to the high level of image noise and clutter. An initial snake closer to the desired boundary is necessary in this case to increase detection accuracy. The BGrad snake, which is represented in red, fails around weak edges causing snake leakages. This is mainly due to the fact that the balloon force is greater than the gradient force. As previously stated in [7], the strength of the balloon force should be manually selected to correctly detect weak edges. Note that our approach, which is represented in green, successfully conforms to the desired boundary with high accuracy for all depicted cases.

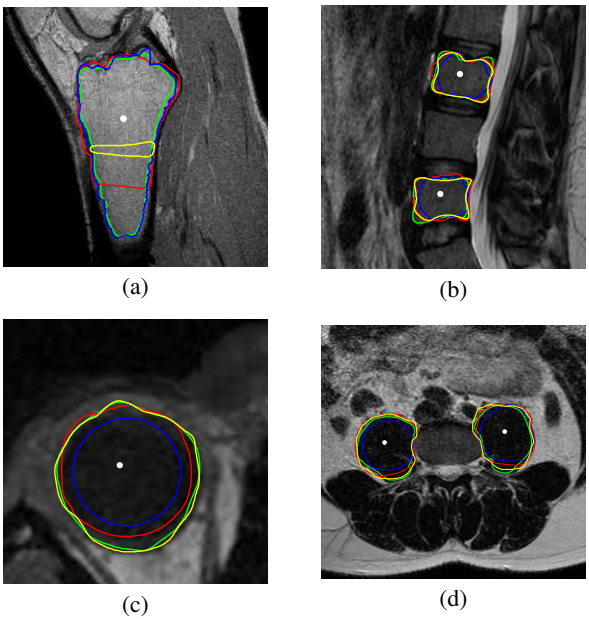

Fig. 5: Final detected boundaries by the GVF snake (yellow), BGrad snake (red), BGVFT snake (blue) and our approach (green). The white dot inside each region represents the manually selected initial position for all evaluated snakes. (a) Experiment 6 - MRI slice of a knee. (b) Experiment 1 (upper region) and experiment 3 (lower region) - an MRI slice of a spinal cord. (c) Experiment 8 - a CT slice of a skull (left eye). (d) Experiment 4 (left region) and experiment 5 (right region)- an MRI slice of a pelvis.

5. CONCLUSION

This paper proposed a novel external force for parametric snakes that combines balloon and GVF forces. The external force uses a weighting factor to leverage the advantages of these two forces according to local image features. In smooth areas with little edge information, balloon forces guide the snake to the object's boundary, while in the presence of strong edge information GVF forces make the snake conform to the boundary. Our proposed approach is compared to snakes using GVF forces, balloon forces and a combination of GVF and balloon forces based on manual thresholding. Experimental results on real medical images show that the proposed external force outperforms the other evaluated external forces, and minimizes snake leakages, while offering the advantage of initializing the snake with a single manually selected point inside the desired region.

6. REFERENCES

[1] Michael Kass, Andrew Witkin, and Demetri Terzopoulos, "Snakes: Active contour models," *International Journal of Computer Vision*, vol. 1, no. 4, pp. 321–331, 1988.

[2] Chenyang Xu and Jerry L Prince, "Snakes, shapes, and gradient vector flow," *IEEE Transactions on Image Processing*, vol. 7, no. 3, pp. 359–369, 1998.

[3] Nikos Paragios and Rachid Deriche, "Geodesic active regions: A new framework to deal with frame partition problems in computer vision," *Journal of Visual Communication and Image Representation*, vol. 13, no. 1, pp. 249–268, 2002.

[4] Yuwei Wu, Yuanquan Wang, and Yunde Jia, "Segmentation of the left ventricle in cardiac cine mri using a shape-constrained snake model," *Computer Vision and Image Understanding*, 2013.

[5] Mengmeng Zhang, Qianqian Li, Lei Li, and Peirui Bai, "An improved algorithm based on the gvf-snake for effective concavity edge detection," *Software Engineering and Applications*, 2013.

[6] Guopu Zhu, Shuqun Zhang, Qingshuang Zeng, and Changhong Wang, "Gradient vector flow active contours with prior directional information," *Pattern Recognition Letters*, vol. 31, no. 9, pp. 845–856, 2010.

[7] Laurent D Cohen, "On active contour models and balloons," *CVGIP: Image understanding*, vol. 53, no. 2, pp. 211–218, 1991.

[8] KW Sum and Paul Cheung, "Boundary vector field for parametric active contours," *Pattern Recognition*, vol. 40, no. 6, pp. 1635–1645, 2007.

[9] Scott T Acton and Nilanjan Ray, "Biomedical image analysis: segmentation," *Synthesis Lectures on Image, Video, and Multimedia Processing*, vol. 4, no. 1, pp. 1–108, 2009.

[10] Lunming Qin, Ce Zhu, Yao Zhao, Huihui Bai, and Huawei Tian, "Generalized gradient vector flow for snakes: New observations, analysis and improvement," *IEEE Transactions on Circuits and System for Video Technology*, vol. 23, no. 5, pp. 883–897, 2013.

[11] Yuhua Yao, Lixiong Liu, Lejian Liao, Ming Wei, Jianping Guo, and Yinghui Li, "Sigmoid gradient vector flow for medical image segmentation," in *11th International Conference on Signal Processing (ICSP)*. IEEE, 2012, vol. 2, pp. 881–884.

[12] Yuanquan Wang, Yuwei Wu, and Yunde Jia, "Shape constraints for the left ventricle segmentation from cardiac cine mri based on snake models," in *Medical Image Analysis in Shape Analysis*. Springer, 2014, vol. 14, pp. 373–412.

[13] Victor Sanchez, Rafeef Abugharbieh, and Panos Nasiopoulos, "3d scalable medical image compression with optimized volume of interest coding," *IEEE Transactions on Medical Imaging*, vol. 29, no. 10, pp. 1808–1820, 2010.

[14] Anca Dima, Michael Scholz, and Klaus Obermayer, "Automatic segmentation and skeletonization of neurons from confocal microscopy images based on the 3-d wavelet transform," *IEEE Transactions on Image Processing*, vol. 11, no. 7, pp. 790–801, 2002.

[15] James E Fowler, "The redundant discrete wavelet transform and additive noise," *IEEE on Signal Processing Letters*, vol. 12, no. 9, pp. 629–632, 2005.

[16] Lee R Dice, "Measures of the amount of ecologic association between species," *Ecology*, vol. 26, no. 3, pp. 297–302, 1945.

[17] Paul Jaccard, *Distribution de la Flore Alpine: dans le Bassin des dranses et dans quelques régions voisines*, Rouge, 1901.